Efficient Iris Identification with Improved Segmentation Techniques

Abhishek Verma and Chengjun Liu

Department of Computer Science
New Jersey Institute of Technology
Newark, NJ 07102, USA
{av56, chengjun.liu}@njit.edu

Abstract: In this paper, we propose and implement an improved iris recognition method based on image enhancement and heuristics. We make major improvements in the iris segmentation phase. In particular, we implement the raised to power operation for more accurate detection of the pupil region. Additionally, with our technique we are able to considerably reduce the candidate limbic boundary search space, this leads to a significant increase in the accuracy and speed of the segmentation. Furthermore, we selectively detect the limbic circle having center within close range of the pupil center. The effectiveness of the proposed method is evaluated on a grand challenge, large scale database: the Iris Challenge Evaluation (ICE) dataset.

1. INTRODUCTION

Over the past decade biometric authentication has become a very active area of research due to the increasing demands in automated personal identification. More recently several new notable techniques and methods with applications to face recognition (Liu & Yang, 2009), (Liu, 2007), (Yang, Liu, & Zhang, 2010), eye detection (Shuo & Liu, 2010) and iris (Verma, Liu, & Jia, 2011) biometrics have been proposed. Among many biometric techniques, iris recognition is one of the most promising approaches due to its high reliability for person identification (Ma, Tan, Wang, & Zhang, 2004).

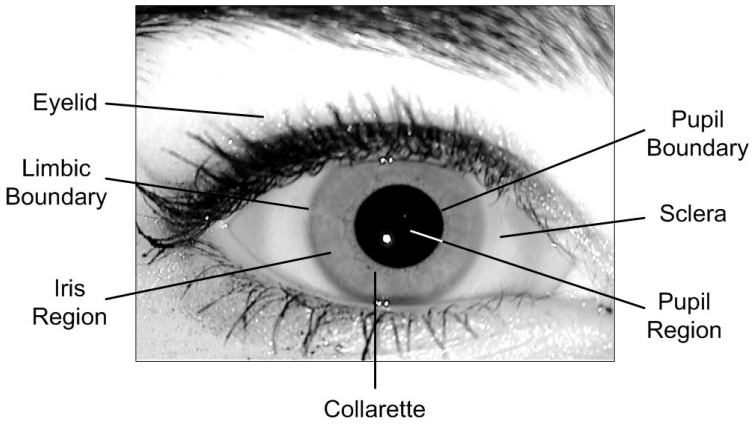

Figure 1. Front view of the human eye. The various parts labeled are important to iris segmentation and recognition.

The iris is a thin circular diaphragm, which lies between the lens and cornea of the human eye. Fig. 1 shows the iris region between the sclera and the pupil. The formation of the unique

patterns of the iris is random and not related to any genetic factors (Wildes, 1997), and the iris patterns remain stable throughout the adult life. Thus, the patterns within the iris are unique to each person and two eyes of an individual have independent iris patterns. Some research shows that when compared with other biometric features such as face and fingerprint, iris patterns are more stable and reliable (Du, Ives, & Etter, 2004).

A general approach to iris recognition consists of four stages: 1) image acquisition, 2) iris segmentation, 3) feature encoding, and 4) decision making. Recent work focuses on handling eye gaze and eyelash exclusion (Daugman, 2007). Bayesian approach to matching of warped iris patterns is discussed by Thornton, Savvides, and Vijayakumar (2007). Beacon guided search for faster iris matching is discussed by Hao, Daugman, and Zielinski (2008) and use of short-length iris codes from the most descriptive regions of the iris for fast iris matching is proposed by Gentile, Ratha, and Connell (2009).

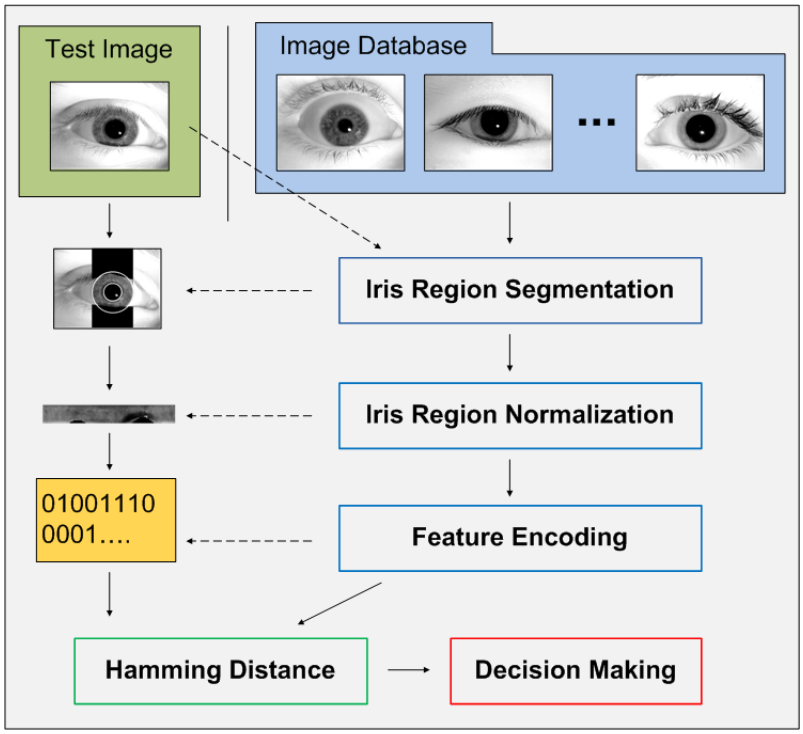

Figure 2. An overview of our iris recognition system.

In this paper, we propose and implement an improved iris recognition method based on image enhancement and heuristics. We make major improvements in the iris segmentation phase. In particular, we implement the raised to power operation for more accurate detection of the pupil region. Additionally, with our technique we are able to considerably reduce the candidate limbic boundary search space, this leads to a significant increase in the accuracy and speed of the segmentation. The segmentation performance is further increased with the application of the thresholding. Furthermore, for higher accuracy and speed, we selectively detect the limbic circle having center within close range of the pupil center. The effectiveness of the proposed method is evaluated on a grand challenge, large scale database: the Iris Challenge Evaluation (ICE) (Phillips, 2006) dataset. The pupil is correctly segmented for 99.8% of the images in the dataset. Iris region detection is 98.5% for the right eye and 98.8% for the left eye. The rank-one recognition rate for our method is 3.5% and 2.7% higher than that of the ICE method for the right eye and the left eye respectively. Furthermore, we improve upon the ND_IRIS (Liu, Bowyer, &

Flynn, 2005) by a significant 2% for the rank-one recognition rate of the left eye. The verification rate is about 10% higher than the ICE method for each eye at a much lower equal error rate; this emphasizes the higher accuracy of our system.

The rest of the paper is structured as follows: In Section 2, we briefly overview several representative works on image acquisition, segmentation, feature encoding and matching. Section 3 describes the dataset used in our experiments along with the implementation details of our improved recognition system. We evaluate the performance of our method and present a detailed analysis of the experimental results in Section 4. Future research directions are discussed in Section 5 and conclusions are drawn in Section 6.

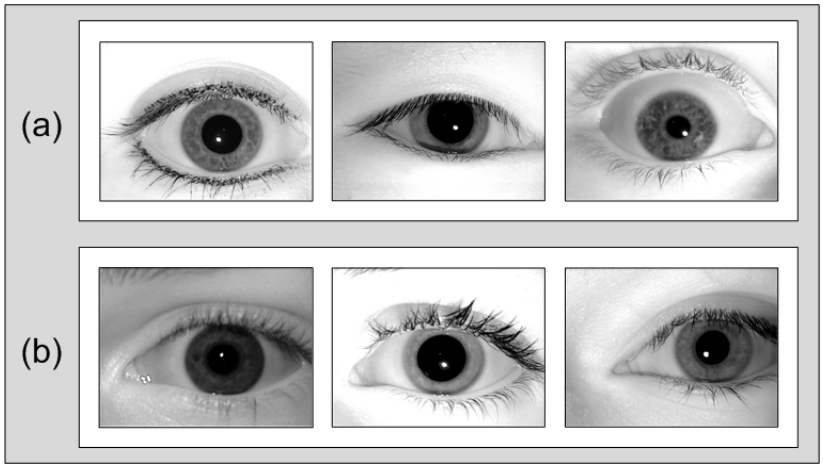

Figure 3. Example images of the (a) right eye and (b) left eye from the ICE dataset, under varying illumination levels, pupil dilation, angle and occlusion.

2. RELATED WORK

Various algorithms have been proposed for iris recognition, one of the earlier systems proposed by Flom and Safir (1987) operates under highly controlled conditions: (i) a headrest is used; (ii) the subject is asked to look at an image in order to stabilize the gaze, and (iii) the process is supervised by an operator. The pupil region is detected by finding large connected regions of pixels with intensity values below a given threshold. In order to extract iris descriptors, the difference operator, edge detection algorithms, and the Hough transform are used.

Most commercial systems implement an algorithm using the iriscodes proposed by Daugman (2004, 2006, & 2007). The system first assesses the focus of the image in real time by looking at the power in the middle and upper frequency bands of the two-dimensional Fourier spectrum. The next step is to segment the iris region in an image, and the early work is based on the assumption that the inner and outer iris boundaries can be modeled as a circle. The more recent work on segmentation relaxes this assumption (Daugman, 2009). After the segmentation of the iris region, the next step describes the features of the iris in a way that facilitates the matching of the two irises. In order to account for variable iris sizes from pupil dilation caused by changes in illumination and camera distance the iris region is mapped into a normalized coordinate system. The rotation of the iris due to the head tilt is accounted for at the stage of matching. The normalized iris image is convolved with the 2D Gabor filters to extract the texture information. After the texture in the image is analyzed and represented, it is matched against the stored representation of other irises. In order to speed up the matching, from the texture features, the phase response of each filter is quantized into a pair of bits. Each complex coefficient is transformed into a two-bit code: the first bit is equal to one if the real part of the coefficient is

positive, and the second bit is equal to one if the imaginary part of the coefficient is positive. Thus, after the quantization the texture of the iris image is summarized in a compact 256 byte binary code. The binary "iriscodes" can be compared efficiently using bitwise operations with a metric called the normalized Hamming distance, which measures the fraction of bits for which the two iriscodes differ. A small Hamming distance suggests strong similarity of the iriscodes.

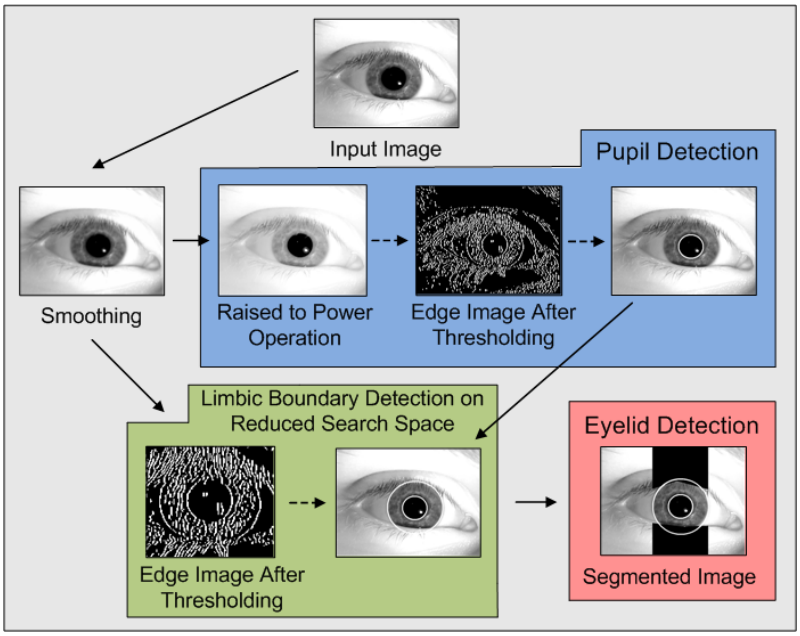

Figure 4. An overview of the three main stages in iris segmentation: the pupil detection, the limbic boundary detection, and the eyelid detection.

The Wildes (1997) system uses low light level camera along with diffuse source and polarization for image acquisition. Such a light source is less-intrusive and designed to eliminate specular reflections. The system involves computing the binary edge map followed by the Hough transform to localize the iris boundary. The detection of eyelid is also incorporated into the system. For matching, it applies the Laplacian of Gaussian filter at multiple scales to produce a template and computes the normalized correlation as a similarity measure.

Tisse, Martin, Torres, & Robert (2002) construct the analytic image (a combination of the original image and its Hilbert transform) to demodulate the iris texture. Huang, Luo, & Chen (2002) perform localization of iris by canny edge detection and integro-differential operator, and encoding was done using Independent Component Analysis (ICA). Masek (2003) performs localization of iris by canny edge detection and circular Hough transform. Encoding was performed by 1D Log-Gabor wavelets and matching was based on hamming distance. Cui et al. (2004) propose a method of iris image synthesis based on the Principal Component Analysis (PCA) and super-resolution. The synthesized image was verified using Daugman's algorithm. Ives, Guidry, & Etter (2004) use histogram based technique to perform encoding. It is a computationally less intensive method when compared with other methods. Experiments were conducted on the CASIA eye image dataset. Liu, Bowyer, & Flynn (2005) propose the ND_IRIS method based on Masek's implementation. This method uses hamming distance to compare two iris templates.

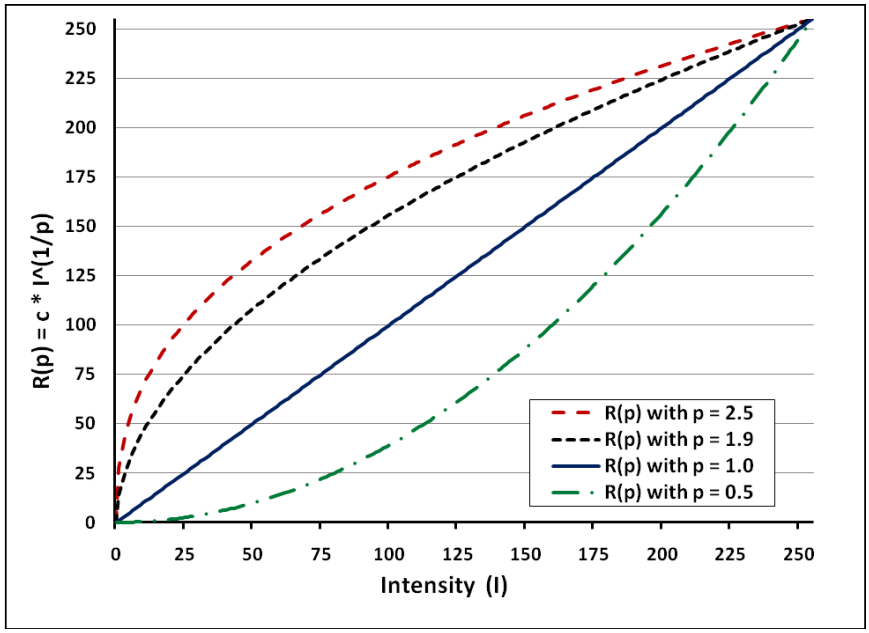

Figure 5. The plot that shows the result of the raised to power operation on the image intensity values at four different *p* values.

3. NEW AND IMPROVED IRIS RECOGNITION METHOD AND ITS MAJOR COMPONENTS

We propose and implement an improved iris recognition method and show the improvement in iris recognition performance using the Iris Challenge Evaluation (ICE) (Phillips, 2006) dataset. First we give details of the ICE dataset in Section 3.1. Next we discuss the major components of our improved iris recognition method. These include iris segmentation, iris encoding, and iris matching. See Fig. 2 for an overview of the iris recognition system.

We focus our efforts mainly on improving the segmentation stage of the system. This allows us to compare the performance of the segmentation stage with that implemented by the ICE method. The segmentation step performs the localization of the iris region by detecting the pupil and the limbic boundary along with the eyelids. The iris encoding and iris matching stage are similar to that implemented by the ICE method in the Biometric Experimentation Environment (BEE) system. Compared to the ICE method our proposed method leads to a significant increase in the accuracy of the iris region segmentation with a much higher overall recognition performance at a lower error rate. Furthermore, our method outperforms the rank-one recognition performance achieved by the ND_IRIS (Liu, Bowyer, & Flynn, 2005) method.

3.1. The ICE Dataset

The ICE dataset consists of 1425 right eye images of 124 different subjects and 1528 left eye images of 120 different subjects. Eye images belong to 132 total subjects with 112 overlapping subjects between the left eye and the right eye images. The iris images are intensity images with a resolution of 640 x 480 in the TIFF format. The average diameter of an iris is 228 pixels. The images vary in quality due to the percent of the iris area occluded, the degree of blur in the image, off angle image, and images with subject wearing the contact lens. Fig. 3(a) shows some example images of the right eye and Fig. 3(b) shows some images from the left eye from the ICE dataset. Notice the varying degree of illumination levels, pupil dilation, angle and occlusion.

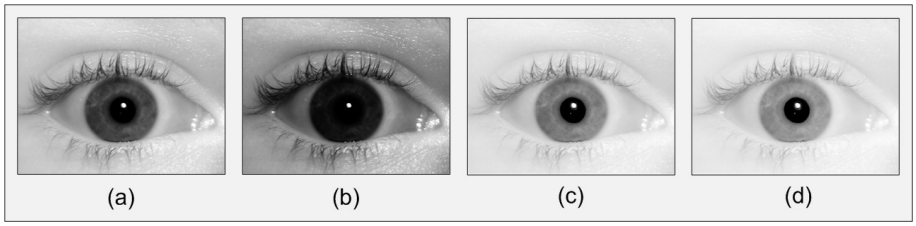

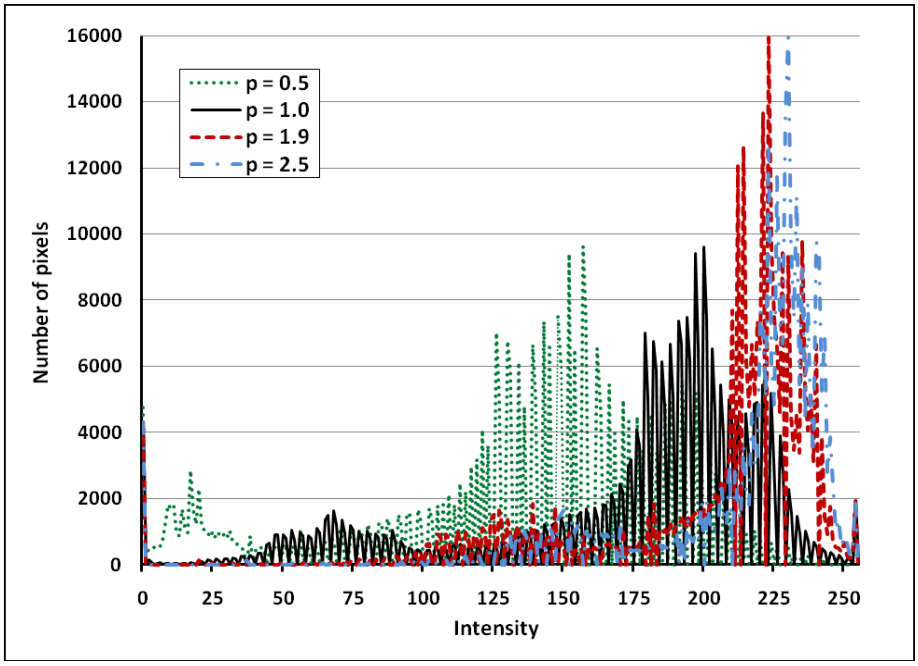

(e)

Figure 6. Results of the raised to power operation on (a) input eye image for p = 0.5, 1.9 and 2.5 shown in (b), (c) and (d) respectively. (e) Plot of the frequency of intensity of the input image at various p values. Plot at p = 1.0 corresponds to the input image in (a).

3.2. Iris Segmentation

Here we give the details of our segmentation method. In particular, we discuss the effect of raised to power operation on an eye image along with its advantages. Next we provide details of efficiently determining the pupil region. Finally, we discuss the method to effectively determine the limbic boundary and the iris region segmentation. See Fig. 4 for an overview of the three main stages in iris segmentation: the pupil detection, the limbic boundary detection, and the eyelid detection.

3.2.1. Performing the Raised to Power Operation on an Eye Image

The raised to power operator when applied to a grayscale image changes its dynamic range. The pixel intensity values in the input image act as the basis which is raised to a (fixed) power. The operator is defined by the following formula (Gonzalez & Woods, 2001):

$$R(p) = c * I^{1/p} \quad (1)$$

where I is the intensity value of a pixel in the input image, c is the scaling factor and $1/p$ is the power.

For $p < 1$, this operation increases the bandwidth of the high intensity values at the cost

of the low pixel values. For $p > 1$, this process enhances the low intensity value while decreasing the bandwidth of the high intensity values, i.e., enhances the contrast in the dark regions. For $p = 1$ the above transformation linearly scales the intensity value.

In Fig. 5 the plot shows the result of the raised to power operation on the image intensity values at four different values of p. The output pixel value is scaled back to the intensity between 0 and 255. This operation when applied on the input pixel intensity with $p = 1$ and $c = 1$ does not have any effect on the output intensity. This can be seen in the plot for $R(p)$ at $p = 1$. For $p = 1.9$ and 2.5 the lower intensity values gain more than the higher intensity values. At $p = 0.5$ the intensity values get pulled down and the lower values tend to get mapped to a narrower range.

We assess the impact of the raised to power operation on an eye image in terms of the pixel intensity frequency in Fig. 6. The original eye image is shown in Fig. 6(a), transformed images with p values as 0.5, 1.9 and 2.5 can be seen in Fig. 6(b), (c) and (d) respectively. The corresponding pixel intensity frequency plot for the four images is presented in Fig. 6(e). For $p > 1$ many more pixels get mapped into a narrower brighter intensity range as seen in Fig. 6(e). Also, this effect can be observed from the eye images in Fig. 6(c) and (d) where the contrast between the pupil and the iris becomes more significant.

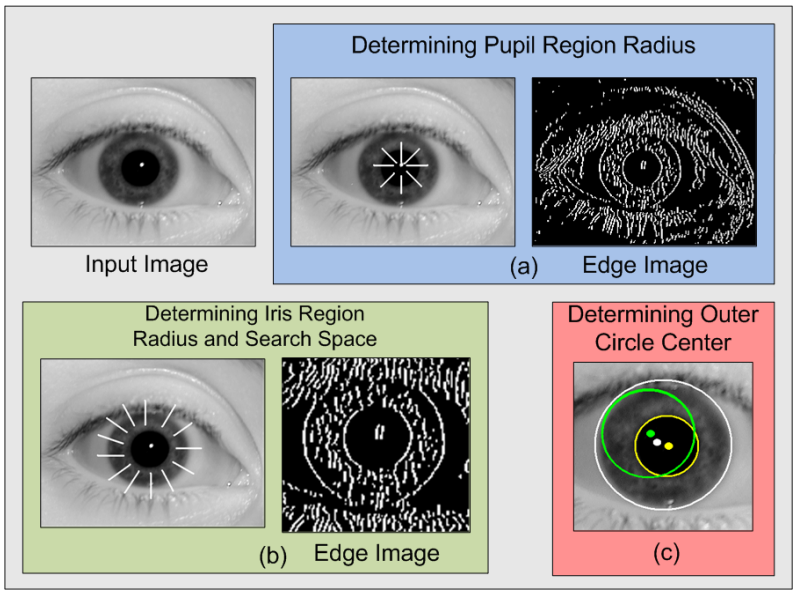

Figure 7. Efficient determination of (a) determining the pupil region radius, (b) determining the iris region radius and search space, and (c) determining the limbic boundary center.

3.2.2. Efficient Determination of the Pupil Region

Our new iris segmentation method first applies the raised to power operation on an eye image and then detects the pupil boundary. We first detect the pupil boundary and then detect the outer iris boundary. The reason for this approach lies in the observation that the contrast between the iris and the pupil is usually larger than that between the iris and the sclera (Liu, Bowyer, & Flynn, 2005). The contrast is further enhanced from the application of the raised to power operation, this makes it easier to detect the pupil region and thereby increases the accuracy of the pupil segmentation. Our method results in the accurate detection of the pupil boundary for 99.8% of the images in the dataset, this includes all the right eye and the left eye images. The appropriate p value for the raised to power operator is selected after analyzing the contrast between the iris and the pupil on a large number of eye images.

In Fig. 4 we present the details of the pupil detection. In order to get rid of the noise, as a

first step we apply the Gaussian filter to smooth the input image. The Gaussian smoothing filter is defined by the following formula (Forsyth & Ponce, 2003):

$$G(x,y) = \frac{1}{2\pi\sigma^2} e^{-\frac{x^2+y^2}{2\sigma^2}} \quad (2)$$

where x is the distance from the origin in the horizontal axis, y is the distance from the origin in the vertical axis, and σ is the standard deviation of the Gaussian distribution. In the next stage, we apply the raised to power operation followed by the canny edge detector to detect edges in the image. Thresholding is performed to get rid of the weak edges.

Finally, we apply the circular Hough transform on the edge image to detect the pupil boundary. In order to make the pupil search more accurate and fast, we search for a candidate pupil having radius within a narrow range. This range is computed from a validation set chosen from the ICE dataset. See Fig. 7(a) image on the left for the range of the radius and on the right the edge image space to be searched for candidate pupil circles. The circular Hough transform can be described as a transformation of a point in the x, y-plane to the circle parameter space. The parametric representation of the circle is given as:

$$\begin{aligned} x &= a + r\cos(\theta) \\ y &= b + r\sin(\theta) \end{aligned} \quad (3)$$

where a and b are the center of the circle in the x and y direction respectively and where r is the radius and θ is the angle between 0 and 2π.

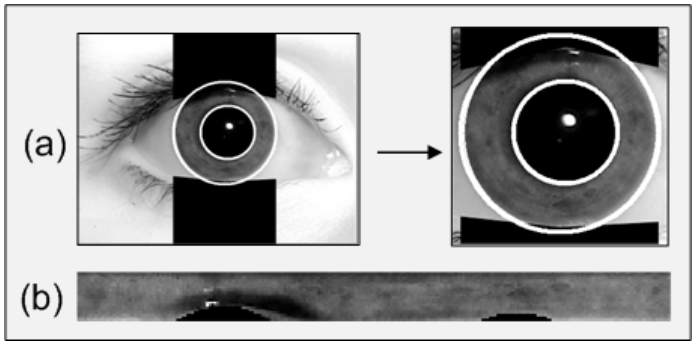

Figure 8. (a) Segmented iris region and (b) its normalized iris region.

3.2.3. Efficient Determination of the Limbic Boundary and the Iris Region

We observe that when detecting the limbic boundary, the Hough transform often makes incorrect detections. Our research reveals that those incorrect detections are due to the presence of a large number of weak edges. Therefore, we apply a thresholding technique on the edge image produced by the Canny edge detector to get rid of the insignificant edge points. This has shown to improve the percentage of the correctly segmented iris region by close to 3% for both the right eye and the left eye images. See Fig. 4 for details.

In order to further improve the accuracy of the Hough transform for detecting the limbic boundary, we search for the circle within a specific region around the detected pupil boundary. Furthermore, we search for a candidate limbic boundary having radius within a narrow range. The range for the radius is estimated on the validation set taken from the ICE dataset. The reduced search space and the narrow radius range thus considerably increase the speed of the circle detection. See Fig. 7(b) left image for the range of the radius and on the right the reduced edge image space that will be searched for candidate limbic circles.

Additionally, we apply another efficient technique to detect the limbic boundary. The Hough transform implemented by the ICE method searches the maximum in the parameter space

to detect the circle. We implement a technique based on the Hough transform that increases the accuracy of the correct limbic boundary detection by 1.3% for the right eye and by 1.4% for the left eye images. Specifically, when the center of the detected circle is farther from the center of the detected pupil by a predefined threshold value, then the detected circle is rejected. Out of all the non-rejected circles we select the one that corresponds to the maximum in the parameter space of the Hough transform and has center coordinates within a predefined threshold value from the pupil center. As a result, our heuristic method considerably increases the accuracy of the Hough transform. In Fig. 7(c) the center for the pupil is pointed in yellow, the incorrect limbic boundary circle with center in green is rejected as it is farther from the pupil center when compared to the correct limbic detection with center displayed in white.

We then model each eyelid as two straight lines. The eyelid detection is implemented by splitting the iris region horizontally and vertically resulting in four equal windows (Liu, Bowyer, & Flynn, 2005). We detect the eyelid in each of these four windows, and connect the results together. Fig. 4 shows the result of the eyelid detection.

3.3. Feature Encoding and Matching

The feature encoding stage encodes the iris image texture patterns into iriscodes using filters. We normalize the iris region to a constant dimension before encoding. Denoising of the noise regions in the normalized pattern is implemented by means of averaging. This results in a bitwise template which contains iris information and a noise mask for corrupt areas within the iris pattern. Fig. 8 shows the result of the normalization of the iris region.

Encoding is implemented by convolving the normalized iris pattern with the 1D Log-Gabor wavelets. The frequency response of a Log-Gabor filter is given as:

$$G(f) = \exp\left(\frac{-(\log(f/f_0))^2}{2(\log(\sigma/f_0))^2}\right) \tag{4}$$

where f_0 represents the centre frequency, and σ gives the bandwidth of the filter. Details of the Log-Gabor filter are given by Field, (1987).

We use the Hamming distance to measure the similarity of the two iris templates. The Hamming distance defines the similarity between two iriscodes, and the two iriscodes are a match when their Hamming distance is close to each other. In comparing the bit patterns X and Y, the Hamming distance (HD) is defined as the sum of disagreeing bits (sum of the XOR between X and Y) over N, the total number of bits in the bit pattern. Below is the formula:

$$HD = \frac{1}{N}\sum_{j=1}^{N} X_j \oplus Y_j \tag{5}$$

Noise bits in the two templates are discarded. The iris template is shifted bit-wise from -15 degrees to +15 degrees with an increment of 1.5 degrees each time, and the Hamming distance is computed for two shift positions. The lowest Hamming distance is the best match between the two templates. Such shifting is necessary to take care of the misalignment in the normalized iris patterns caused by the rotational differences during imaging.

4. EXPERIMENTAL RESULTS

Here we present the details of the experimental evaluation of our proposed method on the ICE dataset. In order for us to make a through comparative assessment of the performance of our method with other methods, we conduct three sets of experiments for the right eye and the left eye. First we assess the correctness of iris segmentation, next we assess the rank-one recognition performance and finally we assess the verification performance for the right eye and the left eye according to the experimental setup proposed by the ICE system. The rank-one recognition criterion and the verification criterion evaluate the performance of our method for recognition

from different viewpoints, we provide more details later in this Section. For all our experiments we scale the input image to 0.4 of its original size, this significantly cuts down the processing time without compromising the correctness of the results.

4.1. Assessing the Correctness of Segmentation

The first set of experiments is designed to assess the correctness of segmentation for the pupil region, the limbic boundary and the iris region on the right eye and the left eye. Considering the nature of the ICE dataset, we now define the correctness of segmentation based on the assumption that the pupil and iris can be modeled as a circle. The pupil region is said to be correctly segmented when the circle fully encloses the pupil region and does not include any area other than the dark pupil. Incorrect pupil segmentation may cover parts of the iris region and or only enclose the pupil region partially. Refer to Section 3.2.2 for the discussion on the method and Fig. 9(c) and (d) for the results. The limbic boundary is said to be correctly segmented when the circle fully bounds the iris region from outside and does not include any area outside of the iris region other than the pupil or the eyelids that may sometimes occlude the iris. Incorrect limbic boundary segmentation may cover parts of the sclera region and or only enclose the iris region partially. Refer to Section 3.2.3 for the discussion on the method and Fig. 10(a) and (b) for the results. The iris region is said to be correctly segmented when for any given eye image both the pupil and the limbic boundary are correctly detected.

TABLE I
Correctness of Segmentation for the
Pupil and Iris Region at Different Values of p

p	Right Eye		Left Eye	
	Pupil Region	**Iris Region**	**Pupil Region**	**Iris Region**
0.7	96.3%	95.5%	96.8%	96.0%
1.0	98.3%	97.4%	98.6%	97.7%
1.3	98.9%	98.0%	99.2%	98.1%
1.6	99.2%	98.2%	99.5%	98.4%
1.9	**99.7%**	**98.5%**	**99.9%**	**98.8%**
2.2	99.6%	98.4%	99.9%	98.8%
2.5	99.6%	98.4%	99.8%	98.7%

In Table I we give the results of the correctness of the pupil and iris region segmentation. The raised to power operation is performed for pupil detection on the right and left eye image at different values of p. At $p = 1$ and $c = 1$ the raised to power operation leaves the intensity values of the pixels in the input image unchanged. For values of $p > 1$, the raised to power operation enhances the contrast in the dark regions and thereby makes the pupil boundary easier to detect. This is confirmed by the percentage of correct pupil detection as p goes higher. Also, for $p < 1$, the contrast between the pupil and the surrounding region decreases making it harder to detect the pupil. We obtain best pupil detection results at $p = 1.9$ with close to 100% correct pupil detection for the left eye and 99.7% for the right eye. For the p values higher than 1.9, we do not notice any significant change in the segmentation performance. The best result for the iris region detection is 98.5% for the right eye and 98.8% for the left eye. The iris region detection is at its highest when the pupil region detection is maximum; this is largely due to the fact that for our method the correct detection of iris region is to an extent dependent on the correct pupil region detection.

Finally, the iris region detection rate at $p = 1.9$ is 1.1% higher for both the right and the left eye when compared with the rate at $p = 1$.

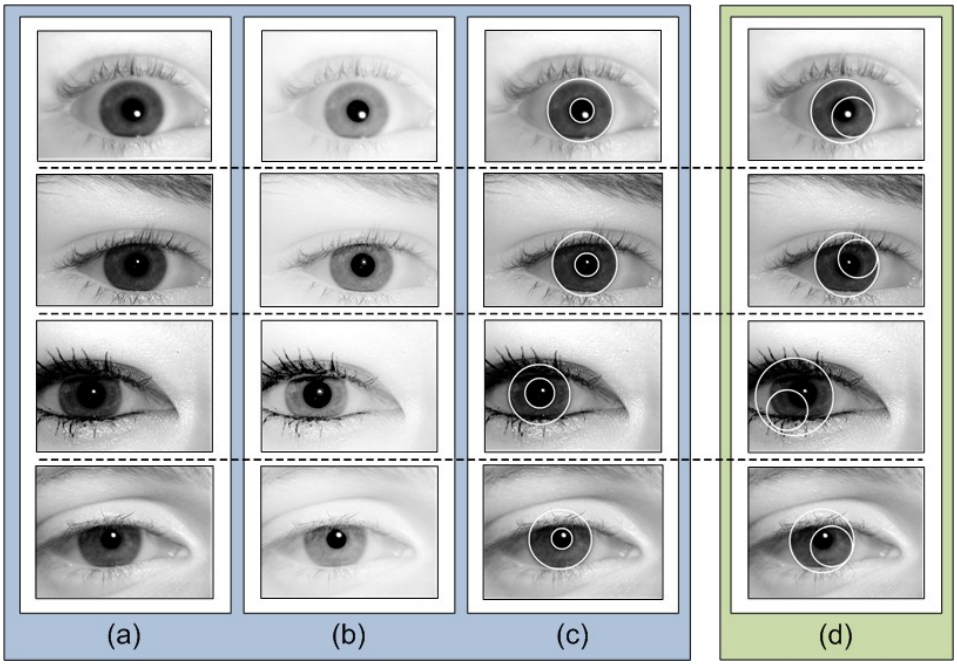

Figure 9. Comparison of the pupil segmentation performance of our improved method with the ICE method. (a) Input eye images, (b) images after the raised to power operation, (c) examples of correct segmentation of the pupil and iris region by our method. (d) Incorrect segmentation by the ICE method.

Fig. 9(c) shows examples the correct segmentation of the pupil based on our improved pupil region detection method. Input images are shown in Fig. 9(a) and the result of the raised to power operation in seen in Fig. 9(b). We compare our results with the incorrect segmentation results by the ICE method in Fig. 9(d). In Fig. 10(a) we present the results of our improved limbic boundary segmentation method and make a comparison with the incorrect limbic boundary detection by the ICE method shown in Fig. 10(b).

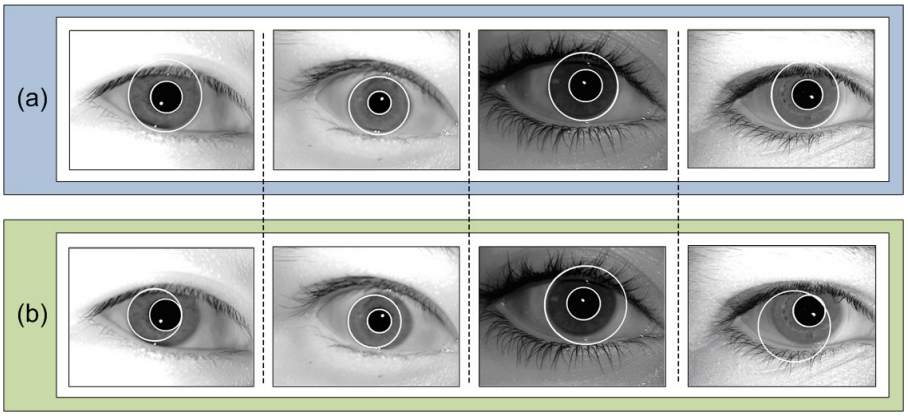

Figure 10. Comparison of the limbic boundary segmentation performance of our improved method with the ICE method. (a) Examples of correct segmentation by our method. (b) Incorrect segmentation by the ICE method.

From Table II it can be seen that our method improves upon the ICE method for pupil

region segmentation by 4.3% and 4.2% for the right eye and the left eye respectively. Our limbic boundary detection rates are higher by 5.3% and 5.4% for the right and left eye respectively. Finally, we improve upon the ICE method by 8.3% for both the right and left eye iris region detection.

TABLE II
Comparison with the Results from the ICE Method of the Correctness of Segmentation for the Pupil Region, Limbic Boundary and Iris Region

	Our Method		**ICE Method**	
	Right Eye	**Left Eye**	**Right Eye**	**Left Eye**
Pupil Region	**99.7%**	**99.9%**	95.4%	95.7%
Limbic Boundary	**98.7%**	**99.0%**	93.4%	93.6%
Iris Region	**98.5%**	**98.8%**	90.2%	90.5%

4.2. Assessment of the Rank-one Recognition Performance

Here we evaluate the effectiveness of our method based on the rank-one recognition rate. This is a popular evaluation criterion for iris recognition. To obtain the recognition rate, we need to first calculate the Hamming distance between every pair of a query image and a target image, and then use the nearest-neighbor classifier for classifying all query images. If the query image and the target image belong to the same subject or class, it is a correct match. The recognition rate is the ratio of the number of correctly classified query images to the total number of query images. The rank-one recognition rate underlines the similarity of the samples that are close to one another within a class.

TABLE III
Rank-one Recognition Performance at Different Values of p

p	**Right Eye**	**Left Eye**
0.7	95.4%	95.9%
1.0	97.6%	98.1%
1.3	98.3%	98.5%
1.6	98.7%	98.8%
1.9	**99.0%**	**99.0%**
2.2	98.9%	99.0%
2.5	98.9%	98.9%

From Table III it can be seen that the best recognition rate is 99% for both the right eye and the left eye at $p = 1.9$, when compared to the rate at $p = 1$, this is higher by 1.4% for the right eye and by 0.9% for the left eye. We do not notice any significant change in the recognition performance for $p > 1.9$.

TABLE IV

Comparison of the Rank-one Recognition
Performance with the Other Methods

	Right Eye	Left Eye
Our Method	**99.0%**	**99.0%**
ND_IRIS	-	97.08%
ICE Method	95.5%	96.3%

The rank-one recognition rate for our method as shown in Table IV is 3.5% and 2.7% higher than that of the ICE method for the right eye and the left eye respectively. Furthermore, we improve upon the ND_IRIS by a significant 2% for the left eye. Please note that the authors in (Liu, Bowyer, & Flynn, 2005) do not report the recognition rate on the right eye.

4.3. Assessment of the Verification Performance and Equal Error Rate (EER)

In our final set of experiments we evaluate the verification performance and compare our results with the ICE method. The ICE protocol recommends using the receiver operating characteristic (ROC) curves, which plot the iris verification rate, i.e., the true accept rate versus the false accept rate (FAR), to report the iris recognition performance. The verification rate is the rate at which a matching algorithm correctly determines that a genuine sample matches an enrolled sample. The equal error rate (EER) is obtained when the FAR equals the false reject rate (FRR). Generally, the lower the EER value the higher is the accuracy of the biometric system.

The ROC curves are automatically generated by the BEE system when a similarity matrix is input to the system. In particular, the BEE system generates two ROC curves, corresponding to the Experiment 1 for the right eye and Experiment 2 for the left eye images. The iris verification rate at the false accept rate of 0.1% is generally used as a standard for performance comparison (Yang, Liu, & Zhang, 2010).

TABLE V
Iris Verification Performance at 0.1%
False Accept Rate and EER at Different Values of *p*

p	Right Eye		Left Eye	
	VR	**EER**	**VR**	**EER**
0.7	85.1%	8.3%	84.7%	7.7%
1.0	91.3%	5.2%	90.9%	4.6%
1.3	92.8%	4.9%	92.2%	4.2%
1.6	94.2%	3.9%	93.3%	3.1%
1.9	**95.1%**	**2.8%**	**94.4%**	**2.3%**
2.2	95.1%	2.8%	94.4%	2.3%
2.5	95.0%	2.8%	94.3%	2.3%

VR is the verification rate and EER is the equal error rate.

It should be pointed out that the verification rate in the ICE Experiment 1 and 2 emphasizes the similarity of samples that are relatively distant from one another within a class because it needs to measure all similarity between samples, whereas the recognition rate

discussed in Section 4.2 emphasizes the similarity of samples that are close to one another within a class since it applies a nearest-neighbor classifier. Therefore, these two criteria evaluate the performance of our method for recognition from two different viewpoints.

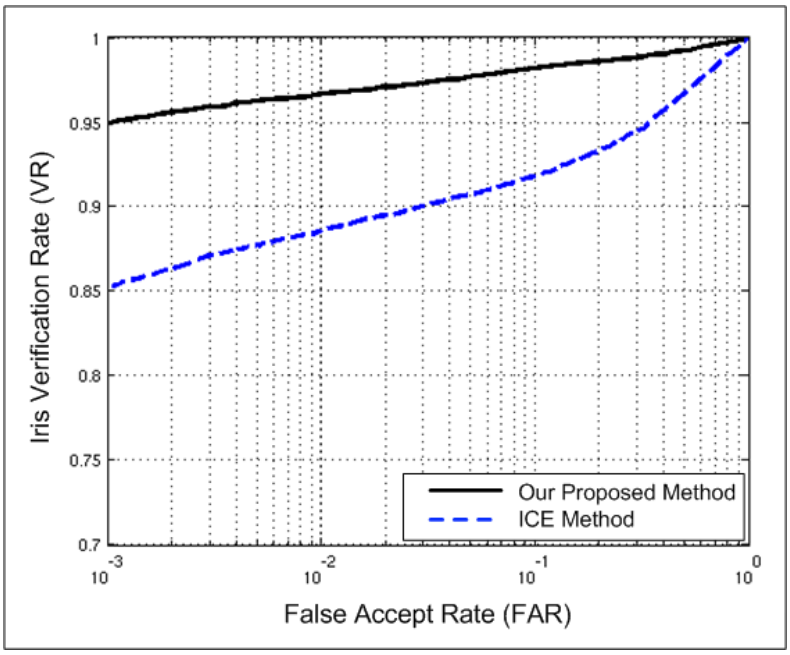

Figure 11. Comparison of the Iris verification performance (ROC curve for the right eye) of the ICE method with our proposed method.

From Table V it can be seen that the best verification rate and the lowest EER is achieved at $p = 1.9$. When compared to the performance at $p = 1$, the VR is higher by 3.8% at a low EER of 2.8% for the right eye and the VR is higher by 3.5% at the EER of 2.3% for the left eye. We do not notice any significant change in the verification performance for $p > 1.9$.

We compare in Fig. 11 and Fig. 12 the performance of our method with that of the ICE method in terms of the ROC curves. Fig. 11 and Fig. 12 show the ROC curves for the right eye experiment and the left eye experiment respectively. It can be observed that our proposed method improves the iris recognition performance significantly in comparison with the ICE method.

TABLE VI
Comparison with the ICE Method on the Iris Verification
Performance at 0.1% False Accept Rate and EER

	Right Eye		**Left Eye**	
	VR	**EER**	**VR**	**EER**
Our Method	**95.1%**	**2.8%**	**94.4%**	**2.3%**
ICE Method	85.2%	8.5%	84.9%	7.8%

VR is the verification rate and EER is the equal error rate.

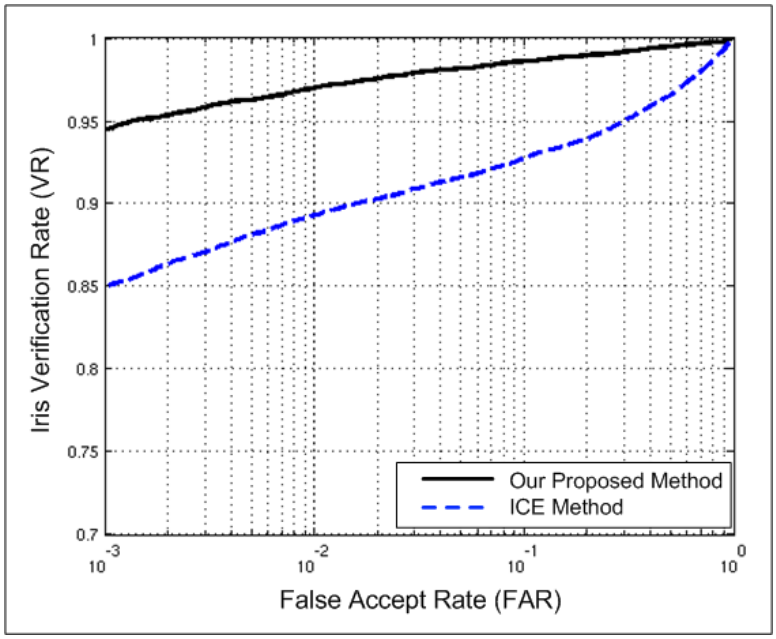

Figure 12. Comparison of the Iris verification performance (ROC curve for the left eye) of the ICE method with our proposed method.

From Table VI it can be seen that our method improves upon the ICE method notably. For the right eye, our proposed method has a verification rate of 95.1%, which is about 10% higher than the ICE method. The EER is 2.8%, which is much lower than the 8.5% for the ICE method. For the left eye, our proposed method has a VR of 94.4%, which is again about 10% higher than the ICE method. The EER is 2.3%, which is much lower than the 7.8% for the ICE method; this emphasizes the higher accuracy of our system.

FUTURE RESEARCH DIRECTIONS

The system presented here was able to perform accurately, however there are still several issues that need to be addressed. In order to make the iris recognition more practical in less-controlled conditions, we need to look at the segmentation of off-angle iris images, images with contacts and blurred images. Our experimental results also suggest that more work is needed on segmentation of the limbic boundary, especially for the iris images with relatively lower quality. In order to make the system for real-time recognition more robust, an indexing scheme based on the color of the iris can be performed, this would allow for faster search and matching.

CONCLUSION

In this paper we presented an improved method for iris recognition with enhanced performance on the ICE dataset. In particular, we implement the raised to power operation for more accurate detection of the pupil region. Additionally, with our technique we are able to considerably reduce the candidate limbic boundary search space, this leads to a significant increase in the accuracy and speed of the segmentation. The segmentation performance is further increased with the application of the thresholding. Furthermore, for higher accuracy and speed, we selectively detect the limbic circle having center within close range of the pupil center. The pupil is correctly segmented for 99.8% of the images in the dataset. Iris region detection is 98.5% for the right eye and 98.8% for the left eye. The rank-one recognition rate for our method is 3.5%

and 2.7% higher than that of the ICE method for the right eye and the left eye respectively. Furthermore, we improve upon the ND_IRIS by a significant 2% on the rank-one recognition rate of the left eye. The verification rate is about 10% higher than the ICE method for each eye at a much lower equal error rate.

REFERENCES

Cui, J., et al. (2004). *An Iris Image Synthesis Method Based on PCA and Super-Resolution.* Int. Conf. on Pattern Recognition, 471-474.

Daugman, J. (2004). *How iris recognition works*. IEEE Trans. on Circuits and Systems for Video Technology, 14(1), 21-30.

Daugman, J. (2006). Probing the uniqueness and randomness of iriscodes: results from 200 billion iris pair comparisons. *Proceedings of the IEEE, 94*(11), 1927-1935.

Daugman, J. (2007). New methods in iris recognition. *IEEE Trans. on Systems, Man and Cybernetics B, 37*(5), 1167-1175.

Du, Y., Ives, R.W., & Etter, D.M. (2004). Iris recognition: A chapter on biometrics. *The Electrical Engineering Handbook*. Boca Raton, FL: CRC Press.

Field, D.J. (1987). Relations between the statistics of natural images and the response properties of cortical cells. *Journal of the Optical Society of America, 4*(12), 2379-2394.

Flom L., & Safir, A. (1987). *Iris recognition system*. U.S. Patent 4,641,349.

Forsyth, D. & Ponce, J. (2003). *Computer Vision: A Modern Approach*. Upper Saddle River, NJ: Prentice Hall.

Gentile, J. E., Ratha, N., & Connell, J. (2009, September). *SLIC: Short Length Iris Code*. International Conference on Biometrics: Theory, Applications and Systems, Washington, D.C.

Gonzalez, C.G. & Woods, R.E. (2001). *Digital Image Processing*. Upper Saddle River, NJ: Prentice Hall.

Hao, F., Daugman, J., & Zielinski, P. (2008). A fast search algorithm for a large fuzzy database. *IEEE Transactions on Information Forensics and Security, 3*(2), 203-212.

Huang, Y., Luo, S., & Chen, E. (2002). *An Efficient Iris Recognition System*. Machine Learning and Cybernetics, 450- 454.

Ives, R.W., Guidry, A.J., & Etter, D.M. (2004). *Iris recognition using histogram Analysis*. Signals, Systems and Computers, 562-566.

Liu, C. (2007). The Bayes decision rule induced similarity measures. *IEEE Transactions on Pattern Analysis and Machine Intelligence, 29*(6), 1116-1117.

Liu, C. & Yang, J. (2009). ICA color space for pattern recognition. *IEEE Transactions on Neural Networks, 20*(2), 248-257.

Liu, X., Bowyer, K.W., & Flynn, P.J. (2005). *Experiments with an Improved Iris Segmentation Algorithm*. Workshop on Automatic Identification Advanced Technologies, 118-123.

Ma, L., Tan, T., Wang, Y., & Zhang, D. (2004). Efficient iris recognition by characterizing key local variations. *IEEE Trans. Image Processing, 13*(6), 739-750.

Masek, L. (2003). *Recognition of human iris patterns for biometric identification.* www.csse.uwa.edu.au/~pk/studentprojects/libor, The University of Western Australia.

Phillips, P.J. (2006). *FRGC and ICE Workshop*. Tech. Report. National Institute of Standards and Technology.

Shuo, C. & Liu, C. (2010, September). *Eye Detection Using Color Information and a New Efficient SVM*. International Conference on Biometrics Theory, Applications and Systems, Washington, D.C.

Thornton, J., Savvides, M., & Vijayakumar, B.V.K. (2007). A Bayesian approach to deformed pattern matching of iris images. *Transactions on Pattern Analysis and Machine Intelligence, 29*(4), 596-606.
Tisse, C., Martin, L., Torres, L., & Robert, M. (2002). *Person Identification Technique Using Human Iris Recognition*. Proc. Vision Interface, pp. 294-299.
Verma, A., Liu, C., & Jia, J. (2011). New color SIFT descriptors for image classification with applications to biometrics. *International Journal of Biometrics, 3*(1), 56-75.
Wildes, R. (1997). Iris recognition: An emerging biometric technology. *Proc. of the IEEE, 85*(9), 1348-1363.
Yang, J., Liu, C., & Zhang, L. (2010). Color space normalization: Enhancing the discriminating power of color spaces for face recognition. *Pattern Recognition, 43*(4), 1454-1466.

ADDITIONAL READING

1. Castleman, K. R. (1996). *Digital image processing*. Upper Saddle River, NJ: Prentice Hall.
2. Jähne B. (1997). *Digital image processing – concepts, algorithms and scientific applications*. Berlin, BE: Springer.
3. Marion, A. (1991). *An introduction to image processing.* New York, NY: Chapman and Hall.
4. Marr, D. (1982). *Vision: a computational investigation into the human representation and processing of visual information*. San Francisco, CA: W. H. Freeman.
5. Trucco, E. and Verri, A. (1998). *Introductory techniques for 3D computer vision*. Upper Saddle River, NJ: Prentice Hall.
6. Vapnik, V. N. (2000). *The nature of statistical learning theory*. New York, NY: Springer-Verlag.

KEYWORDS AND DEFINITIONS

1. *Image Enhancement* – Improving the interpretability or perception of information in images for human viewers or as an input for automated image processing techniques.
2. *Raised to Power Operation* – Transforming the intensity of an image through power operation.
3. *Image Segmentation* – Changing the representation of a digital image by partitioning the image into multiple segments for simpler and easier analysis.
4. *Heuristics* – Set of exploratory problem-solving methods that utilizes learning techniques by the 'discovery method' to improve performance.
5. *ICE* – Iris Challenge Evaluation
6. *Iris Recognition* – Method of biometric authentication that uses pattern-recognition techniques based on high-resolution images of the irises of an individual's eyes.
7. *Biometrics* – Methods for uniquely recognizing humans based upon one or more inherent physical or behavioral traits.